JOURNAL OF SOLID STATE CHEMISTRY 99, 1–11 (1992)

Structural Phase Transitions of Fast Lithium Ion Conductors $Li_2M^{II}Cl_4$ (M^{II} = Mg, Mn, Cd)

H. J. STEINER AND H. D. LUTZ

Universität Siegen, Anorganische Chemie I, Postfach 101240, W 5900 Siegen, Germany

Received August 8, 1991; in revised form November 26, 1991; accepted December 5, 1991

The order–disorder phase transitions of spinel-type (I) chlorides $Li_2M^{II}Cl_4$ (M^{II} = Mg, Mn, Cd) to Li_2MnBr_4 *cF*56 (II) and disordered, deficient NaCl structure (III) at elevated temperatures are characterized by X-ray diffraction, dilatometry, thermoanalytical, and Raman spectroscopic studies, and are discussed with respect to cation distribution, lithium ion motion, anharmonic interaction of vibrational modes, and order parameters. Full formation of the ordered NaCl superstructure (II) occurs at 360°C for both Li_2MgCl_4 and Li_2MnCl_4. Mn^{2+}-rich $Li_{2-2x}Mn_{1+x}Cl_4$ solid solutions probably possess a Li_2MnBr_4 *cF*56-type structure even at ambient temperatures. In the case of Li_2CdCl_4, disorder of II to III starts before complete depopulation of the tetrahedral 8*a* site of the spinel structure is reached. Disorder to III is finished at 540, 465, and 380°C, respectively. Because of the high defect concentrations and coupling of several ordering processes, one-component Landau theory gives only an unsatisfactory description of the microscopic processes.

Introduction

Ternary lithium chlorides $Li_2M^{II}Cl_4$ and $Li_{2-2x}M^{II}{}_{1+x}Cl_4$ have been reported to be fast lithium ion conductors (*1–5* and references cited therein). The stoichiometric spinel-type compounds $Li_2M^{II}Cl_4$ *cF*56 (M^{II} = Mg, Mn, Cd) (space group $Fd\bar{3}m$) possess an inverse distribution of the metal ions according to $(Li)^t[Li\ M^{II}]^oCl_4$ (I) with lithium on both tetrahedral and octahedral sites (*6–8*). The deficient spinel-type compounds $Li_{2-2x}M^{II}{}_{1+x}Cl_4$ with vacancies on tetrahedral sites (*7*) show an enhanced conductivity (*3, 9–11*). Increasing temperature causes a gradual migration of the lithium ions from tetrahedral 8*a* sites to interstitial octahedral 16*c* positions (of the cubic closed-packed framework of the chloride ions) (*5, 7, 12, 13*), i.e., the spinel structure transforms to an ordered NaCl defect structure (Li_2MnBr_4 *cF*56 type (*14*), space group $Fd\bar{3}m$) (II). Subsequently, high-temperature disordered NaCl defect-structure polymorphs (space group $Fm\bar{3}m$, *cF*7) (III) are formed by isomorphic and class-equivalent (klassengleiche) transformations, respectively (*11*). (A similar spinel to NaCl defect-structure disorder transition has been reported for $FeYb_2S_4$ (*15*).)

As a consequence of the order–disorder transitions, the mobility of the lithium ions (*5*) and, hence, the ionic conductivity are strongly enhanced. Therefore, a detailed analysis of the order–disorder transitions including the change of the cation distributions should give more information on the microscopic structure and the ionic motion. A useful tool in determining microscopic order parameters is hard mode Raman spec-

0022-4596/92 $5.00

troscopy (*16, 17*). The same holds true for determination of the entropy of the order–disorder transitions. Additionally, X-ray diffraction, calorimetric (DSC), and dilatometric methods are used to characterize the temperature evolution of macroscopic features. Furthermore, we discuss the question whether the order–disorder transitions established can be described by the phenomenological Landau theory of structural phase transitions (*18*).

Within the framework of Landau's theory (*16, 18*) the free energy can be described as a function of the long-range order parameter Q. The thermal behavior of Q follows the expression $Q \sim Q_0|T - T_c|^\beta$ with Q_0, the order parameter in the ordered phase, T_c, the critical temperature, at which the disordered polymorph is formed completely, and β, the critical exponent. $\beta = \frac{1}{2}$ means an ideal Landau behavior, $\beta = \frac{1}{4}$ indicates a tricritical behavior, which is a result of order-parameter coupling, and values of $\beta < \frac{1}{4}$ are only possible for partially first-order phase transitions.

In the case of second-order order–disorder transitions maximum configurational entropy can be estimated from the classical limit $\Delta S = R \cdot \ln(W_2/W_1)$. (Although the temperature evolution of ΔS depends on the transition mechanism (*18*).) W is the number of configurations in the ordered (W_1) and disordered state (W_2). For both spinel-type to Li_2MnBr_4 *cF*56-type and Li_2MnBr_4 *cF*56-type to NaCl defect-structure transitions W_2/W_1 should be 2. In the former case, the lithium ions occupy the tetrahedral 8*a* sites (spinel structure) fully and half of the octahedral 16*c* sites (Li_2MnBr_4 *cF*56 structure) at random. In the latter case, the number of available octahedral lattice sites for the manganese ions is twice as large in the NaCl defect structure as in the Li_2MnBr_4 *cF*56 structure.

Temperature evolution of Raman bands (both frequencies and halfwidths) reveals the change of cation distribution and lattice sites involved as well as dynamical interactions between the lattice modes (*11, 13, 19*). Group theoretical treatment of the lattice vibrations of the ternary chlorides under study yields five Raman allowed modes (species $A_{1g} + E_g + 3F_{2g}$) in the case of spinel structure (space group $Fd\bar{3}m$) and four bands ($A_{1g} + E_g + 2F_{2g}$) for Li_2MnBr_4 *cF*56-type compounds ($Fd\bar{3}m$) (*13, 19*). Additionally, so-called hopping modes have been established (*13, 19*).

Experimental Methods

The ternary chlorides were prepared by fusing appropriate amounts of anhydrous $M^{II}Cl_2$ (M^{II} = Mg, Mn, Cd) and LiCl in evacuated sealed borosilicate glass ampoules (*1, 20, 21*). Single crystals of Li_2MnCl_4 were grown from the melt according to the method of Tammann (*22*) and Stöber as reported elsewhere (*1, 8*). The ternary lithium chlorides are extremely hygroscopic and, hence, they must be handled under a dry argon atmosphere.

The chlorides obtained were characterized by X-ray and high-temperature X-ray Guinier powder technique. Details are reported elsewhere (*21*). The intensities of the X-ray reflections were determined densitometrically (Kipp & Zonen DD2 densitometer).

The thermal expansion of Li_2MnCl_4 single crystals was determined by push-rod dilatometric measurements (for experimental details see (*23*)) using Al_2O_3 stamps and Pt-foils to avoid a reaction of Al_2O_3 with the sample.

Thermoanalytical and calorimetric data were obtained by means of difference-scanning calorimetry (DSC) (Perkin–Elmer DSC 7). Transition enthalpies were determined by using the melting enthalpy of indium as a reference. For further experimental details see (*11, 19*).

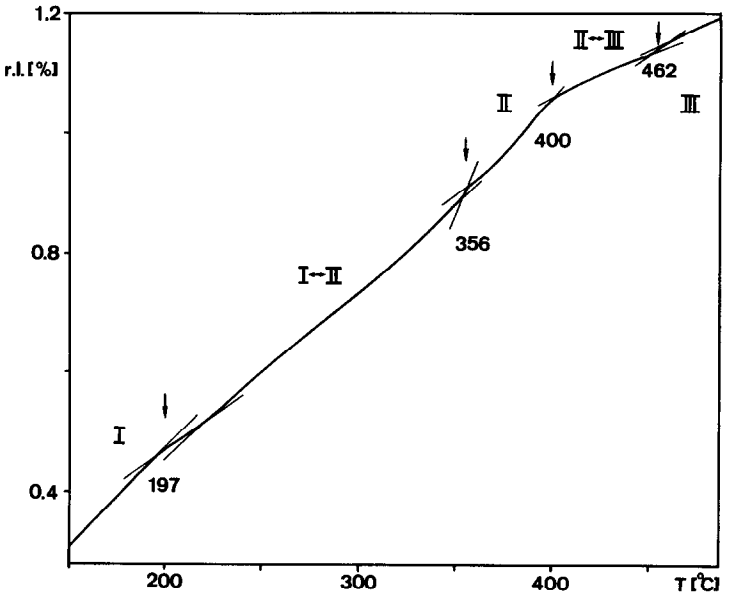

FIG. 1. Change of the relative length (r. l.) of Li_2MnCl_4 single crystals with increase in temperature (dilatometric measurements): I, spinel; II, Li_2MnBr_4 *cF*56; III, disordered, deficient NaCl structure; I–II, etc., temperature regions of continuous phase transitions; ↓, transition temperatures [°C] (for the linear expansion coefficient see (*19*)).

The Raman spectra, with samples taken in sealed glass capillaries, were recorded on a Dilor OMARS 89 multichannel Raman spectrograph (spectral slit width <4 cm^{-1}). For excitation the 514.5-nm line of an Ar^+ ion laser was employed. Details of the high-temperature measurements are given elsewhere (*13, 24*).

Results

Dilatometric measurements of Li_2MnCl_4 single crystals reveal continuous phase transitions from spinel via Li_2MnBr_4 *cF*56 to NaCl defect structure (see Fig. 1). The thermal expansion observed resembles the results of high-temperature X-ray diffraction studies (see Fig. 2). Because the thermal expansions obtained from both dilatometry and X-ray studies coincide, the order–disorder transitions cannot be of Schottky type, but of Frenkel type, as proposed earlier from neutron-diffraction studies (*7, 12*).

The relative intensity of the superlattice reflection 311 (spinel and Li_2MnBr_4 *cF*56 type) decreases with increase in temperature owing to the transition from space group $Fd\bar{3}m$ to $Fm\bar{3}m$ (NaCl defect structure) (see Fig. 3). This intensity decrease is a suitable order parameter in the framework of Landau's theory (*18*).

DSC measurements of $Li_2M^{II}Cl_4$ and $Li_{2-2x}Mn_{1+x}Cl_4$ show some broad endothermic features below the melting temperature above 500°C (see Figs. 4 and 5, and Table I), indicating the phase transitions mentioned above. The transition temperatures of $Li_{2-2x}Mn_{1+x}Cl_4$ solid solutions observed confirm those reported by Kanno *et al.* (*3, 10*). The lack of an endothermic peak at about 300°C in the case of $Li_{1.6}Mn_{1.2}Cl_4$ indicates the different structure of this Mn^{2+}-

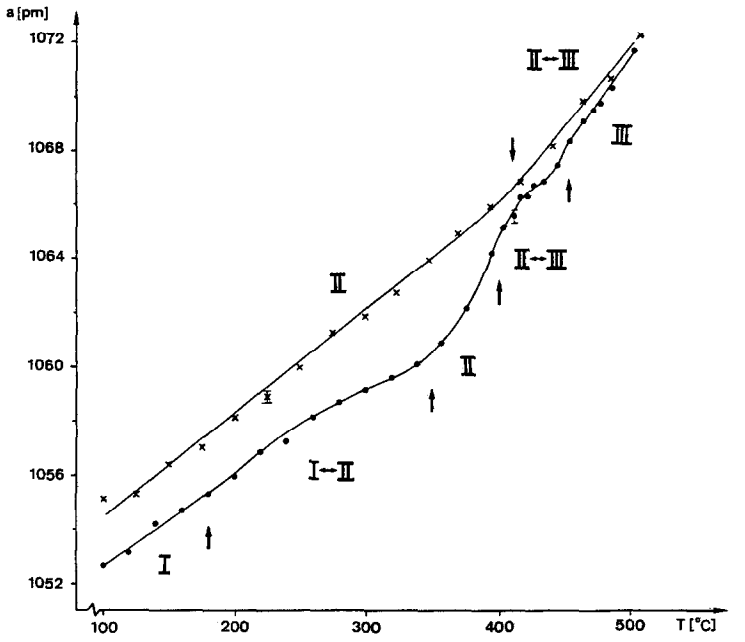

FIG. 2. Temperature evolution of lattice constant a of Li_2MnCl_4 (●) and $Li_{1.6}Mn_{1.2}Cl_4$ (×); ↑, phase transitions (for further explanations see Fig. 1).

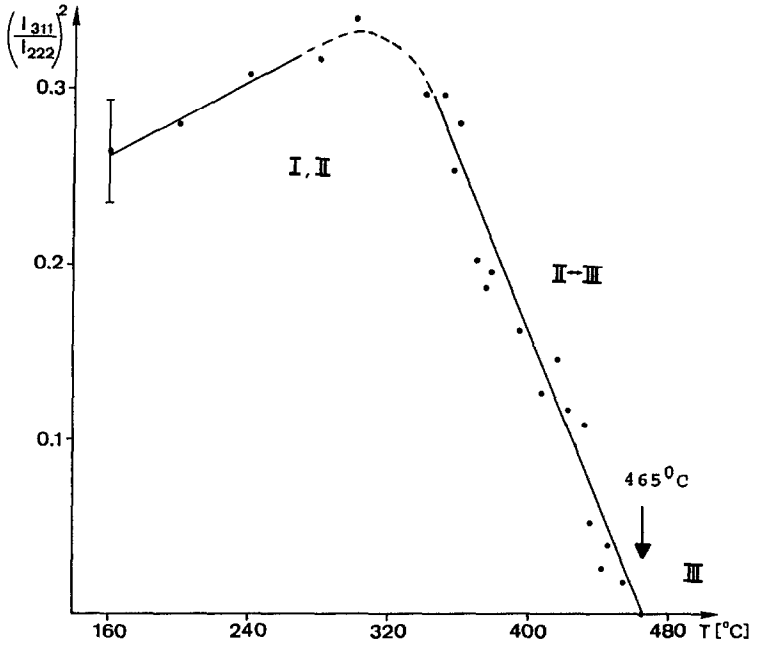

FIG. 3. Temperature evolution of the relative intensity of the 311 superlattice reflection of Li_2MnCl_4: $(I_{311}/I_{222})^2$ vs. temperature (for further explanations see Fig. 1).

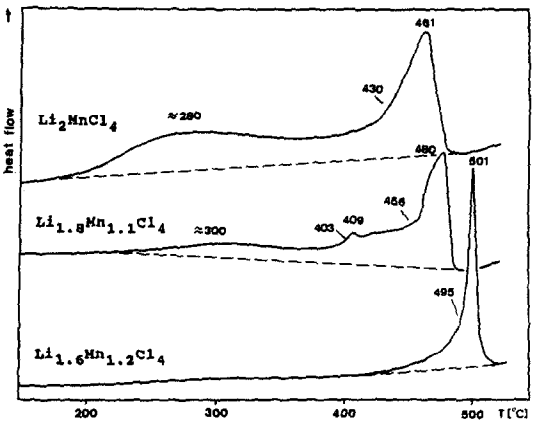

FIG. 4. DSC heating curves (10°C/min) of $Li_{2-2x}Mn_{1+x}Cl_4$ (x = 0, 0.1, 0.2) (see also (*3*, *10*)): temperatures (onset, peak) [°C]; ---, base lines (for enthalpy and entropy data see Table I).

rich solid solution (Li_2MnBr_4 *cF*56 type instead of inverse spinel structure) and, hence, the nonexistence of a spinel to Li_2MnBr_4 *cF*56-type phase transition. In the case of Li_2CdCl_4, the spinel to Li_2MnBr_4 *cF*56-type and Li_2MnBr_4 *cF*56 to NaCl defect-type phase transitions partly overlap (see Fig. 5). Consequently, the Li_2MnBr_4

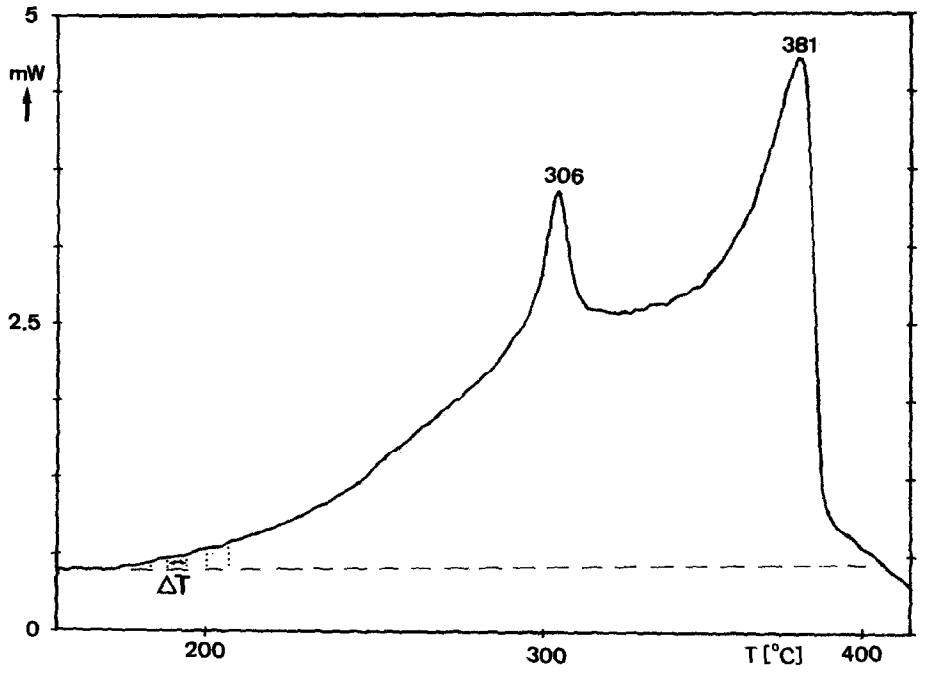

FIG. 5. DSC heating curve of Li_2CdCl_4 (see also (20)): ΔT, temperature steps for calculation of the transition entropies (for further explanations see Fig. 4).

TABLE I

DSC DATA OF THE PHASE TRANSITIONS OF $Li_2M^{II}Cl_4$ (M^{II} = Mg, Mn, Cd) AND $Li_{2-2x}Mn_{1+x}Cl_4$ (I, SPINEL TYPE; II, Li_2MnBr_4 *cF*56 TYPE; III, NaCl DEFECT TYPE)

Phase transition	Temperature [°C] Onset	Peak	Enthalpy [kJ mol^{-1}]	Entropy[a] [J mol^{-1} K^{-1}]
Li_2MnCl_4				
I → II	—	280 ± 10	3.1	5.7 ± 0.5
II → III	430 ± 10	461 ± 2	3.2	4.4 ± 0.5
$Li_{1.8}Mn_{1.1}Cl_4$				
I → II	—	300 ± 10	0.9	1.6 ± 0.5
	403 ± 1	409 ± 1		
II → III			≈5.4	7.3 ± 0.5
	456 ± 1	480 ± 1		
$Li_{1.6}Mn_{1.2}Cl_4$				
II → III	495 ± 2	501 ± 1	≈5.5	7.2 ± 0.5
Li_2MgCl_4				
I → II	—	270 ± 10	2.9	5.4 ± 0.5
II → III	511 ± 1	542 ± 2	3.1	4.0 ± 0.5
Li_2CdCl_4				
I → II	—	306 ± 2		
			≈6.6	11.0 ± 1.0
II → III	—	381 ± 2		

[a] Entropies of transition were calculated by summing up of the entropy increase within temperature steps of 5 K (see Fig. 5).

*cF*56-type polymorph is not completely formed before disorder to deficient NaCl structure starts.

Numerical evaluation of the DSC measurements (see Table I) result in 11 ± 1 J mol^{-1} K^{-1} for the whole transition entropy of Li_2CdCl_4. In the case of Li_2MnCl_4 and Li_2MgCl_4, the entropies for the spinel to Li_2MnBr_4 *cF*56-type transition (I → II) have been determined separately, viz. 5.4 ± 0.5 (Li_2MgCl_4) and 5.7 ± 0.5 J mol^{-1} K^{-1} (Li_2MnCl_4). These values nicely resemble the ideal configurational entropy ($R \cdot \ln 2$) of 5.76 J mol^{-1} K^{-1}. This entropy change is assumed to be owing to fully occupied tetrahedral 8*a* positions in the case of the spinel structure compared to only half at random occupied octahedral 16c positions in the case of the Li_2MnBr_4 *cF*56 structure. Furthermore, the temperature dependence of occupation of the corresponding 8*a* and 16*c* positions can be calculated from the experimental data assuming that domains of spinel and Li_2MnBr_4 *cF*56 structure are formed (see Fig. 6).

The migration of Li^+ from tetrahedral 8*a* sites to octahedral 16*c* sites (transition I → II) is also shown by the low-energy shift of the Raman-allowed phonon modes, particularly that of species A_{1g} (see Figs. 6 and 7). (For Li_2MnCl_4 the A_{1g} and E_g Raman modes of the spinel form partly overlap, so that the respective bands cannot be separated (*19*).) In the case of nonstoichiometric $Li_{1.6}Mn_{1.2}Cl_4$, both the low-energy shift (247 (Li_2MnCl_4) → 235 cm^{-1}) and the nearly linear temperature dependence of the A_{1g} mode (see Fig. 7) confirm the findings discussed

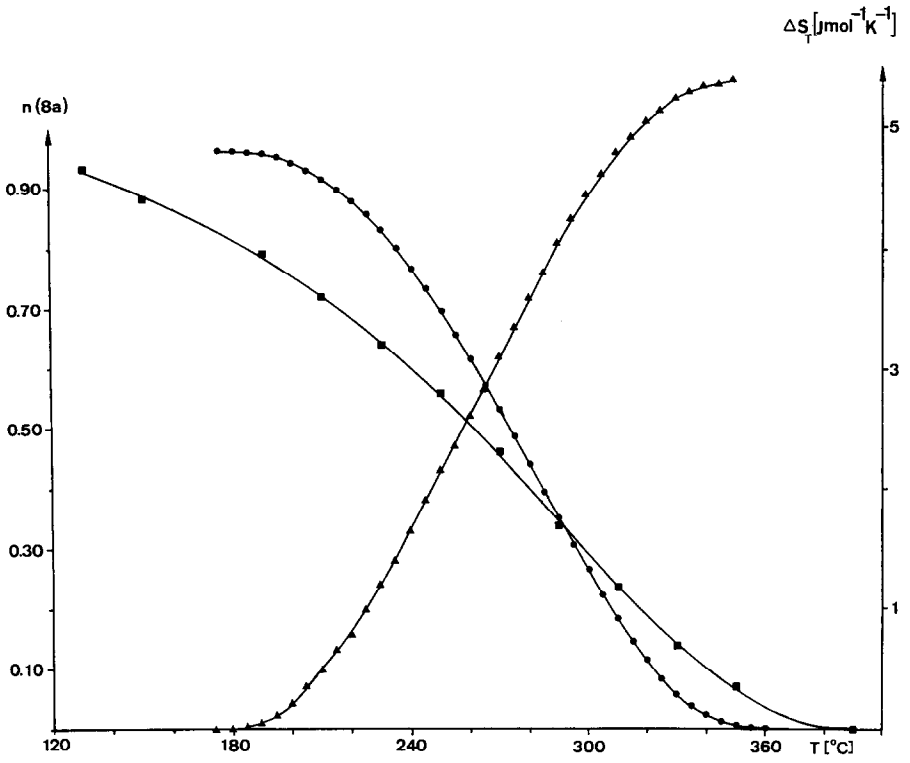

FIG. 6. Occupation of the 8*a* position (spinel structure) of Li_2MgCl_4 as a function of temperature: ●, determined from experimental entropy ΔS_T (▲); ■, from the frequency of the A_{1g} Raman mode (see Fig. 7); for neutron-diffraction data see (7). For these calculations it is assumed that (i) the summed up entropy ΔS_T is due to the amount of spinel-type domains replaced by those of Li_2MnBr_4 *cF*56 structure according to $\Delta S_T = R \cdot \ln (2 - n(8a))$ and (ii) $\tilde{\nu}_{A_{1g}}$ decreases linearly with decrease in $n(8a)$.

above, viz., that these solid solutions possess a Li_2MnBr_4 *cF*56-type structure even at ambient temperature. An Arrhenius plot of full width at half maximum (FWHM) of the A_{1g} mode of Li_2MgCl_4 exhibits well-defined regions of phase stability and phase transformation, as shown from the magnitude of the activation energies (see Fig. 8).

The temperature evolution of the A_{1g} mode frequency of Li_2MgCl_4 (see Fig. 9) corresponds to a slightly first-order phase transition below 263°C (T_{c1}) ($\Delta\tilde{\nu} \sim Q^2$, $\beta = \frac{1}{8}$). Between 263 and 360°C (T_{c2}), at which the Li_2MnBr_4 *cF*56-type polymorph is completely formed, the square of the frequency shift gives a better fit ($\beta = \frac{1}{4}$, "tricritical" region).

Discussion

The phase transitions from spinel to Li_2MnBr_4 *cF*56 structure exhibits a "tricritical" behavior of the order parameter in the microscopic Raman spectroscopic picture (see Fig. 9). The temperature evolution of the FWHM values of the Raman bands is mainly influenced by perturbation of translational symmetry and anharmonic interaction of the lattice modes (*11, 19*) ("vibrational dephasing" (*25, 26*)). The activation

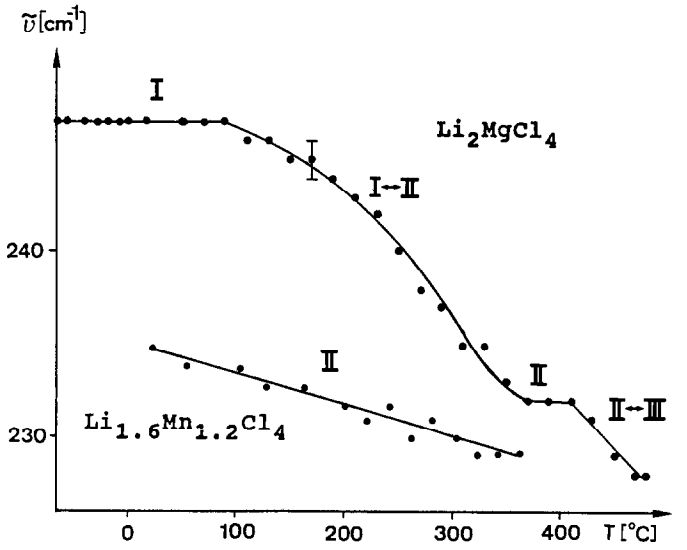

FIG. 7. Temperature evolution of the frequency of the A_{1g} lattice mode of Li_2MgCl_4 and $Li_{1.6}Mn_{1.2}Cl_4$ (for further explanations see Fig. 1; for complete Raman spectra of $Li_2M^{II}Cl_4$ see (*13, 19, 20*)).

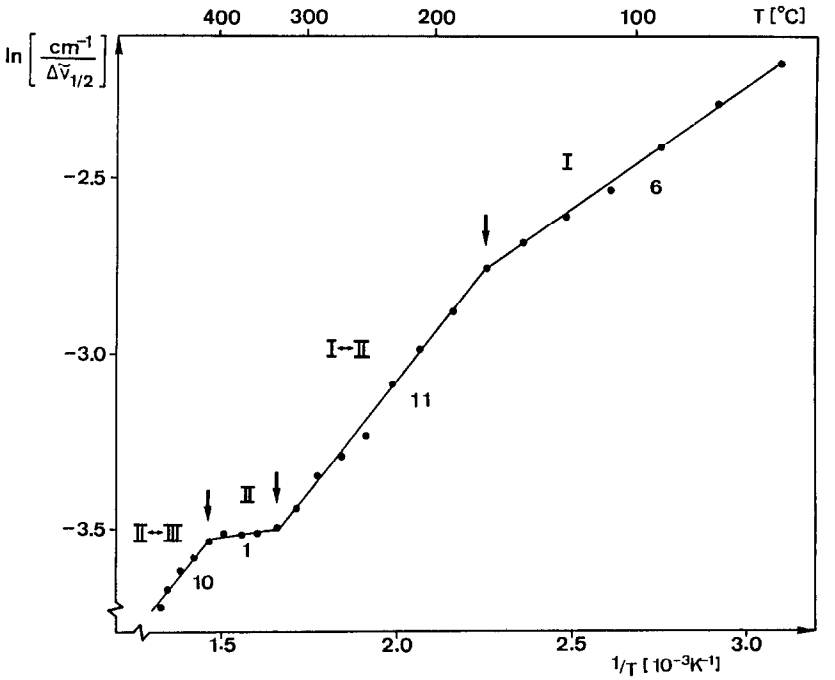

FIG. 8. Arrhenius plot of full width at half maximum of the A_{1g} mode of Li_2MgCl_4; numbers: activation energies [kJ mol^{-1}] (for further explanation see Fig. 1).

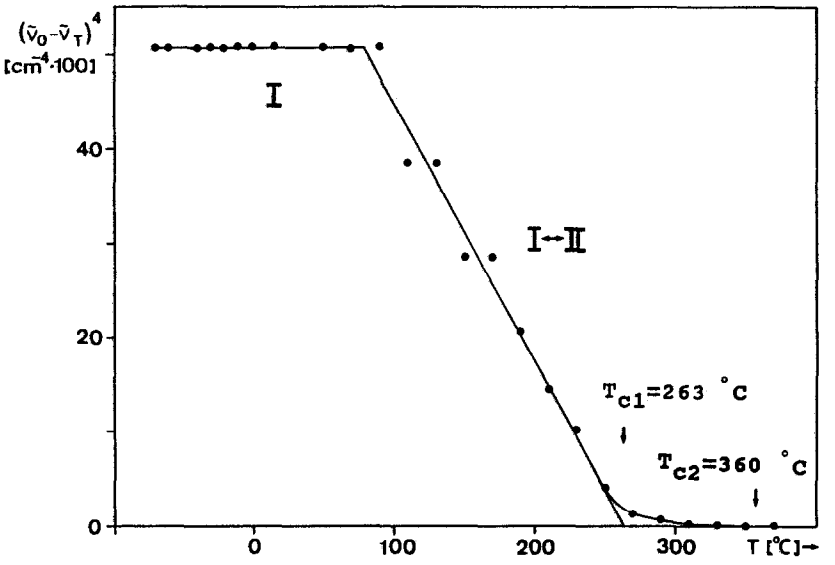

FIG. 9. Landau-like behaviour of the A_{1g} mode of Li_2MgCl_4: $\tilde{\nu}_0$ means the frequency of the ordered spinel-type phase; above T_{c1} $(\tilde{\nu}_0 - \tilde{\nu}_T)^2$ leads to a better fit (for further explanations see text and Fig. 1).

energies in the monophase regions (see Fig. 8) are typical of such anharmonic interactions.

The relative intensity of the superlattice Bragg reflections (spinel and Li_2MnBr_4 *cF*56 type) describes the temperature evolution of the *macroscopic* order parameter in the framework of Landau's theory (*18*). The square of the measured intensity of the superlattice reflection 311 of Li_2MnCl_4 (spinel and Li_2MnBr_4 *cF*56 type) normalized at the fundamental reflection 222 corresponds to Q^4 (see Fig. 3). This likewise means a "tricritical" behavior ($\beta = \frac{1}{4}$) (*27*) with a critical temperature of 465°C (T_{c3}) for the "class-equivalent" Li_2MnBr_4 *cF*56 to NaCl defect-type phase transition.

From the temperature evolution of the amount of spinel-like cation distribution in the structure follows that several partly counteracting ordering and disordering processes occur (S-form of the curves shown in Fig. 6). As calculated from the configurational entropy (see Fig. 6), occupation of the 8*a* and 16*c* sites with equal parts of lithium ions is obtained at 270 and 285°C for Li_2MgCl_4 (see Fig. 6) and Li_2MnCl_4, respectively. In the case of Li_2MgCl_4, neutron-diffraction studies (*7*) revealed the same lithium ion distribution at about 330 ± 30°C. Whether there really exist domains of spinel and Li_2MnBr_4 *cF*56 structure (as assumed for calculation of the occupation of the 8a position from experimental entropy) or there is a random distribution of the lithium ions at the lattice sites involved cannot be decided.

Because at higher temperatures the Li_2MnBr_4 *cF*56-type polymorph becomes more stable as compared to the spinel form, the increasing population of octahedral 16*c* interstitial sites (with respect to the spinel structure) is driven by both entropic and energetic contributions. However, solely the energetic term can give rise to the formation of full Li_2MnBr_4 *cF*56-type polymorphs at 360°C (T_{c2}) for both Li_2MgCl_4 and Li_2MnCl_4. In the case of Li_2CdCl_4, entropy-

driven disordering between the octahedral 16*c* and 16*d* sites, i.e., formation of a disordered NaCl defect structure, starts before complete depopulation of the tetrahedral 8*a* sites is reached. For Li_2MgCl_4 and Li_2MnCl_4 disorder to NaCl defect structure starts at 410 and 400°C, respectively. It is finished at 540 and 465°C, and in the case of Li_2CdCl_4 at 380°C.

The knees in the Arrhenius plots of the electric conductivity, at which the activation energies of conduction strongly decrease (*1–3, 10, 28*), fall into the temperature ranges of the spinel to Li_2MnBr_4 *cF*56-type phase transitions. The temperatures reported, i.e., about 300°C for all Li_2MgCl_4, Li_2MnCl_4, and Li_2CdCl_4, which differ somewhat in the various studies, obviously correspond to those of random distribution of the lithium ions on the 8*a* and 16*c* lattice sites (see above). At these temperatures disorder of the lithium ions is sufficient for a low-activation-energy ionic motion (*28*).

The nonstoichiometric compounds are better lithium ion conductors than the stoichiometric chlorides (*3*). This is owing to the more similar energies of the octahedral 16*c* interstitial and tetrahedral 8*a* lattice sites in the case of the nonstoichiometric compounds (see also the discussion given in (*5*)). Highly nonstoichiometric $Li_{1.6}Mn_{1.2}Cl_4$ probably possess a Li_2MnBr_4 *cF*56-type structure even at ambient temperatures. This is revealed from the absence of spinel to Li_2MnBr_4 *cF*56-type transition as found by X-ray, Raman, and thermoanalytic studies. Contrary to these findings, the likewise nonstoichiometric $Li_{1.33}Mg_{1.33}Cl_4$ has been found to be an inverse spinel by neutron powder diffraction studies (*7*). In general, both the nonstoichiometric managanese and magnesium chlorides $Li_{2-2x}M^{II}{}_{1+x}Cl_4$ tend to form Li_2MnBr_4 *cF*56-type structures with increasing x and at lower temperatures as the stoichiometric spinels.

Acknowledgments

The authors thank Professor Dr. R. Blachnik and Dr. E. Irle, Universität Osnabrück, for their help with the dilatometric measurements, and the Deutsche Forschungsgemeinschaft and the Fonds der Chemischen Industrie for financial support.

References

1. H. D. Lutz, W. Schmidt, and H. Haeuseler, *J. Phys. Chem. Solids* **42,** 287 (1981).
2. R. Kanno, Y. Takeda, and O. Yamamoto, *Mater. Res. Bull.* **16,** 999 (1981).
3. R. Kanno, Y. Takeda, K. Takada, and O. Yamamoto, *J. Electrochem. Soc.* **131,** 469 (1984).
4. R. Kanno, Y. Takeda, and O. Yamamoto, *Solid State Ionics* **28–30,** 1276 (1988).
5. H. D. Lutz, P. Kuske, and K. Wussow, *Solid State Ionics* **28–30,** 1282 (1988).
6. C. J. J. Van Loon and J. De Jong, *Acta Crystallogr. Sect. B: Struct. Crystallogr. Cryst. Chem.* **B31,** 2549 (1975).
7. J. L. Soubeyroux, C. Cros, Wang Gang, R. Kanno, and M. Pouchard, *Solid State Ionics* **15,** 293 (1985).
8. H. D. Lutz and M. Schneider, *Z. Naturforsch. B: Anorg. Chem. Org. Chem.* **45B,** 1543 (1990).
9. R. Kanno, O. Yamamoto, C. Cros, and J. L. Soubeyroux, *Nato ASI Ser. Ser. E.* **101,** 460 (1985).
10. R. Kanno, Y. Takeda, O. Yamamoto, C. Cros, Wang Gang, and P. Hagenmuller, *Solid State Ionics* **20,** 99 (1986).
11. H. D. Lutz, W. Schmidt, and H. J. Steiner, *Z. Anorg. Allg. Chem.*, **604,** 39 (1991).
12. H. D. Lutz, P. Kuske, and A. Pfitzner, *Ber. Bunsenges. Phys. Chem.* **93,** 1340 (1989).
13. K. Wussow, H. Haeuseler, P. Kuske, W. Schmidt, and H. D. Lutz, *J. Solid State Chem.* **78,** 117 (1989).
14. H. D. Lutz, J. K. Cockcroft, P. Kuske, and M. Schneider, *Mater. Res. Bull.* **25,** 451 (1990).
15. L. Ben-Dor, I. Shilo, and I. Felner, *J. Solid State Chem.* **28,** 363 (1979).
16. Z. Iqbal, *in* "Vibrational Spectroscopy Of Phase Transitions" (Z. Iqubal and F. J. Owens, Eds.), p. 1, Academic Press, Orlando, San Diego (1984).
17. U. Bismayer, *Phase Transitions* **27,** 211 (1990).
18. E. K. H. Salje, B. Wruck and H. Thomas, *Z. Phys. B: Condens. Matter* **82B,** 399 (1991).
19. H. J. Steiner, Thesis, University of Siegen (1991).
20. H. D. Lutz, W. Schmidt, and H. Haeuseler, *Z. Anorg. Allg. Chem.* **453,** 121 (1979).
21. H. D. Lutz, K. Wussow, and P. Kuske, *Z. Naturforsch. B: Anorg. Chem. Org. Chem.* **42B,** 1379 (1987).

22. G. TAMMANN, "Lehrbuch der Metallographie," Leopold Voss, Leipzig and Hamburg (1914).
23. W. F. HEMMINGER AND H. K. CAMMENGA, "Methoden der thermischen Analyse," Springer-Verlag, Berlin, Heidelberg (1989).
24. K. BECKENKAMP, Thesis, University of Siegen (1991).
25. C. B. HARRIS, R. M. SHELBY, AND P. A. CORNELIUS, *Phys. Rev. Lett.* **38,** 1415 (1977).
26. T. E. JENKINS AND J. LEWIS, *J. Raman Spectrosc.* **11,** 1 (1981).
27. W. W. SCHMAHL AND E. SALJE, *Phys. Chem. Miner.* **16,** 790 (1989).
28. W. SCHMIDT AND H. D. LUTZ, *Ber. Bunsenges. Phys. Chem.* **88,** 720 (1984).